Kinetic Analysis of the Calmodulin-Binding Region of the Plasma Membrane Calcium Pump Isoform 4b†

Alan R. Penheiter,‡,§ Adelaida G. Filoteo,‡ John T. Penniston,‡,|| and Ariel J. Caride*,‡

Department of Biochemistry and Molecular Biology, Mayo Clinic, 200 First Street SW, Rochester, Minnesota 55901, and Laboratory of Membrane Biology, Neuroscience Center, Massachusetts General Hospital, 55 Fruit Street, Boston, Massachusetts 02114

Received June 3, 2004; Revised Manuscript Received November 9, 2004

ABSTRACT: The sequence L_{1086}RRGQILWFRGLNRIQTQIKVVKAFHSS$_{1113}$ (peptide C28) is responsible for calmodulin binding to PMCA4b. In this work, peptides following the above sequence were progressively shortened either at the N-terminus (C28NΔ3, C28NΔ5, or C28NΔ6) or at the C-terminus (C20, C22, C23, and C25). Competitive inhibition of PMCA activity was used to measure apparent dissociation constants of the complexes between calmodulin and C28 or progressively shortened peptides. Additionally, equilibrium titrations were used to measure the apparent dissociation constants of the various peptides with TA-calmodulin by changes in TA-calmodulin fluorescence and Trp fluorescence of the peptides. At the N-terminus, deletion of five residues did not change calmodulin affinity, but deletion of six residues resulted in a 5-fold decrease in affinity. There were no major differences in the time course of TA-CaM binding, but C28NΔ6 exhibited a different time course of Trp fluorescence change. At the C-terminus, deletion of five residues (C23) or more resulted in a net increase in fluorescence of TA-CaM upon binding, while longer peptides (C25 and C28) produced both a transient increase and a net decrease in the fluorescence of TA-CaM. Global regression analysis revealed that binding of TA-CaM to the C23 peptide could be fit by a two-step model, while longer peptides required three-step models for adequate fitting. TA-calmodulin dissociated rapidly from C23, C22, and C20, resulting in a marked increase in apparent K_d. Thus, the sequence I_{1091}LWFRGLNRIQTQIKVVKAF$_{1110}$ (C25NΔ5) is required to reproduce the calmodulin-binding properties of C28. When F_{1110} was replaced by A, the TA-calmodulin association and dissociation kinetics resembled C23 kinetics, but changing V_{1107} to A produced a smaller effect, suggesting that F_{1110}, rather than V_{1107}, is the main anchor for the N-terminal lobe of calmodulin in PMCA4b.

Calmodulin (CaM)[1] provides the main regulation for the plasma membrane calcium pumps (PMCAs). Both the maximal activity and the affinity for Ca^{2+} are increased by CaM (*1*). In the past few years, attention has come to a special feature of PMCA activation by CaM. The PMCA activation is slow, and the rate of this activation varies with PMCA isoforms (*2*). In turn, this slow activation by CaM was shown to be important in determining the rate of activation by Ca^{2+} (*3*). Moreover, since dissociation of CaM is also slow, some isoforms of PMCA react faster to later spikes during repetitive Ca^{2+} stimulation than to an isolated single spike, generating what was termed "memory effect" (*4*). This complex regulation not only has been observed "in vitro" but also was shown to shape the Ca^{2+} signal in cells (*5*). All of these experimental facts emphasize the importance of understanding the mechanisms of CaM activation in PMCA.

CaM activates PMCA by binding within a 28-residue region near the C-terminus (*6*). Work with synthetic peptides (*7*) and truncated constructs (*8*) demonstrated that this region acts both by binding CaM and as an autoinhibitor of the pump.

TA-CaM is a fluorescent derivative that has been used to study the mechanism of CaM binding of several CaM-dependent enzymes (*9*, *10*). Recently, we published a paper in which we analyzed the binding of TA-CaM both to the whole PMCA4b and to the isolated CaM-binding peptide (C28). On the basis of those results we proposed a kinetic mechanism for the activation of PMCA by CaM (*11*). Here we determined, by competition studies as well as by stopped-flow studies with TA-CaM, the boundaries of the CaM-binding region and the role of particular residues, namely, W_{1093}, V_{1106}, and F_{1110}, on CaM binding.

EXPERIMENTAL PROCEDURES

Isolation of Purified hPMCA4b. Human PMCA4b was purified from erythrocyte cells using calmodulin affinity chromatography as previously described (*12*, *13*). The purified samples were stored in liquid nitrogen until use.

† With support from American Heart Association Grant 30531Z to A.J.C. and from NIH Grant GM 28835 to J.T.P.

* To whom correspondence should be addressed. Tel: 507-284-9651. Fax: 507-284-2384. E-mail: caride@mayo.edu.

‡ Mayo Clinic.

§ Present address: Department of Anesthesiology, Mayo Clinic, 200 1st St. SW, Rochester, MN 55901.

|| Massachusetts General Hospital.

[1] Abbreviations: CaM, calmodulin; TA-CaM, 2-chloro-(ϵ-amino-Lys75)-[6-[4-(*N*,*N*-diethylamino)phenyl]-1,3,5-triazin-4-yl]-labeled calmodulin; PMCA, plasma membrane calcium pump; PMCA4b, isoform 4b of the plasma membrane calcium pump.

10.1021/bi0488552 CCC: $30.25
Published on Web 01/22/2005

Measurement of the Calcium ATPase Activity. The binding competition between the purified pump and the peptide for calmodulin was monitored radiometrically by measuring the release of $[^{32}P]P_i$ upon ATP hydrolysis. The protocol followed the method as described. Concentrations of purified pump, calmodulin, and peptides are described in the figure legends. Precautions were taken in the manner and order of addition of calmodulin, peptide, and PMCA to prevent peptides from nonspecifically adhering to tube surfaces. Basically, the peptide was added into the reaction mix that already contains calmodulin and PMCA, and then the resultant mixture was preincubated for 3 min at 37 °C before the reaction was started by adding ATP. The apparent dissociation constant (K_{eq}) for a given peptide was determined by fitting the equation previously described (*13*) to the experimental data.

Binding of Peptides to TA-Calmodulin. Binding of peptides to calmodulin was determined using TA-CaM. Equilibrium binding was assessed by following the fluorescence changes induced by the addition of different peptides to 34 nM TA-CaM in media containing 30 mM Tes−TEA, pH 7.2, 120 mM KCl, 5 mM $MgCl_2$, 0.2 mM EGTA, and enough $CaCl_2$ to obtain 100 μM free Ca^{2+}. Fluorescence was measured in a Varian Cary Eclipse spectrofluorometer. The excitation wavelength was 370 nm, and the emission wavelength was 420 nm.

Stopped-flow measurements of changes in fluorescence of TA-CaM were performed in an Applied Photophysics SX.18MV reaction analyzer, as described in ref *11*, except that the temperature was 12 °C. The lower temperature was adopted to slow the reaction, thereby improving the time resolution. The excitation wavelength was 365 nm, and the emitted light was detected using a 395 nm cutoff filter. The syringes contained 34 nM TA-calmodulin and 400 nM peptide prepared in a media containing 30 mM Tes−TEA, pH 7.2, 120 mM KCl, 5 mM $MgCl_2$, 0.2 mM EGTA, and enough $CaCl_2$ to obtain 100 μM free Ca^{2+}.

Rate of Dissociation of Peptides from TA-Calmodulin. Conditions were similar to those used to measure the rate of binding of TA-CaM. Syringe 1 contained 34 nM TA-calmodulin and 400 nM peptide in the media described before. Syringe 2 contained 2 μM unlabeled calmodulin in the same media.

Changes in Trp Fluorescence. Binding of calmodulin-binding peptides to calmodulin produces a blue shift in the emitted fluorescence of a Trp residue present in these peptides. To follow the kinetics of this change, excitation light was set at 295 nm, and the emitted fluorescence was measured with a 335 nm cutoff filter. Measurements were done in the media described above for experiments using TA-CaM. Final concentrations were 0.5 μM peptides and 2 μM calmodulin.

Origin and Preparation of Reagents. TA-CaM was synthesized and purified as described (*9*). Experiments in this paper were done with TA-CaM prepared with batch II of TA-Cl, which is devoid of contaminants (*9*, *14*). The peptides used in this study were synthesized in the Mayo Protein Core Facility and purified to homogeneity by HPLC. The sequence of each of the peptides is shown in Figure 1.

Analysis of the Results. The experiments were performed at least in triplicate. Individual curves were fitted by nonlinear regression by means of Graphpad Prizm software. When global nonlinear regression was applied to fit a proposed model to progress curves obtained at different concentrations, Dynafit software (Biokin, Inc.) (*15*) was used.

```
                              SEQUENCE OF PEPTIDES
   -
          1        10        20
          1         1         1
C28       LRRGQILWFRGLNRIQTQIKVVKAFHSS
C25       LRRGQILWFRGLNRIQTQIKVVKAF___
C23       LRRGQILWFRGLNRIQTQIKVVK_____
C22       LRRGQILWFRGLNRIQTQIKVV______
C20       LRRGQILWFRGLNRIQTQIK________
C28NΔ3    ___GQILWFRGLNRIQTQIKVVKAFHSS
C28NΔ5    _____ILWFRGLNRIQTQIKVVKAFHSS
C28NΔ6    ______LWFRGLNRIQTQIKVVKAFHSS
C25NΔ5    _____ILWFRGLNRIQTQIKVVKAF___
C28W/A    LRRGQILAFRGLNRIQTQIKVVKAFHSS
C28F/A    LRRGQILWFRGLNRIQTQIKVVKAAHSS
C28V/A    LRRGQILWFRGLNRIQTQIKAVKAFHSS
```

FIGURE 1: Sequence of the peptides used in this study. Residues in peptides are numbered starting from Leu_1, which corresponds to Leu_{1086} in the sequence of PMCA4b.

Modeling the Structure of the Calmodulin−C28 Complex. A structure for the complex was generated from the known structures of calmodulin complexed with calmodulin-binding peptides from nitric oxide synthase (1NIW), calmodulin kinase IIa (1CM1), myosin light chain kinase (2BBM), and C20 from PMCA (a representative structure from 1CFF). The C-terminal half of 1CFF was not considered in generating the structure, since C20 did not bind to that lobe of calmodulin. An alignment was prepared in which the anchor residues of C28 (determined in this study) were aligned with the anchor residues determined for the peptides in each of the structures mentioned above. The structural model of the C28−calmodulin complex was calculated using Modeller 6v2. The figure was made using Deep View v3.7 and POV-Ray 3.5.

RESULTS

In Figure 2 the effects of N-terminal and C-terminal deletions on the affinity for calmodulin are reported. The K_d values obtained by competitive inhibition of ATPase activity are summarized in Table 1. It is easy to see that up to five residues can be removed from the N-terminus without significant change in calmodulin affinity (peptide C28NΔ5). Deletion of six residues from the N-terminus (C28NΔ6) decreases 5 times the affinity for calmodulin. On the other hand, deletion of up to three residues from the C-terminal end of C28 has no significant effect on calmodulin affinity. Deletion of five residues from this end reduces calmodulin affinity about 5-fold, and deletion of a sixth residue produced an even more dramatic effect (20-fold).

To analyze the role of different residues on the kinetics of calmodulin binding, we titrated a fluorescent derivative of calmodulin (TA-CaM) with each of the peptides used in this study. The results are shown in Figure 3 and summarized

Table 1: Parameters from Competition Experiments and Equilibrium Titrations

peptide	K_{eq} from competition (nM)	kinetics type	K_{d1}	K_{d2}	F(TA-CaM−P)/ F(TA-CaM) ratio
C28	0.69 ± 0.15	simple	4.9 ± 2.4		0.10
C25	0.81 ± 0.26	simple	9.0 ± 4.1		0.04
C23	4.5 ± 1.0	simple	444 ± 96		1.89
C22	20.3 ± 6.1	simple	64 ± 39		1.6
C20		double	95 ± 11	169 ± 128	2.71
NΔ5C25		simple	12 ± 7		0.24
NΔ5C28	0.89 ± 0.44	simple	4.9 ± 4.0		0.32
NΔ6C28	4.99 ± 0.85	double	3.1 ± 1.5	226 ± 78	0.53
C28F/A		simple	10 ± 9		1.7
C28V/A		simple	48 ± 27		0.63
C28W/A		complex			1.26

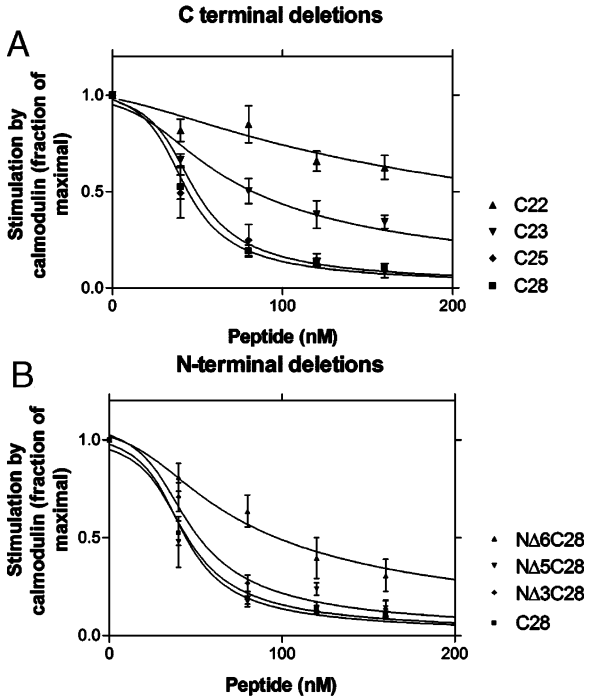

FIGURE 2: Determination of K_d between CaM and different CaM-binding peptides by competitive inhibition of PMCA ATPase activity. Panel A: Peptides with C-terminal deletions. Panel B: Peptides with N-terminal deletions. Inhibition of the ATPase activity and estimation of K_ds were done as described in Experimental Procedures. The experiments were performed in the presence of 17 nM PMCA and 47.8 nM CaM. The free Ca^{2+} concentration was 10 μM.

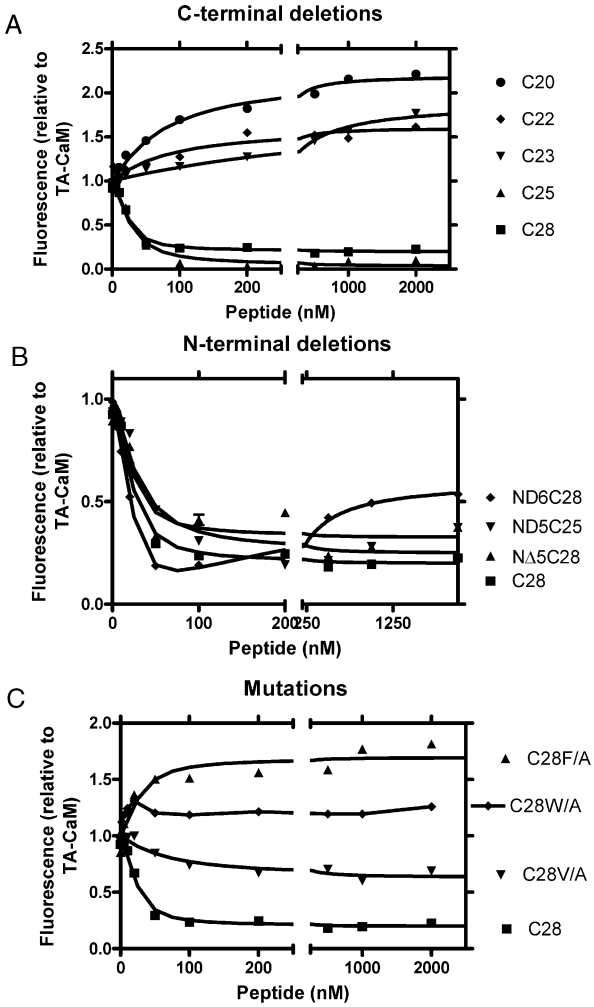

FIGURE 3: Equilibrium titrations of TA-CaM with the peptides used in this study. Panel A shows the peptides with C-terminal deletions, panel B shows the peptides with N-terminal deletions, and panel C shows the peptides with mutations. C28 was included in all three panels for comparison.

in Table 1. Binding of peptides C28, C25, NΔ5C28, and NΔ5C25 resulted in a similar decrease in TA-CaM fluorescence. The results are compatible with binding to one class of sites (K_d = 5−10 nM). Peptides C23, C22, and C28F/A produced an increase in TA-CaM fluorescence, and the kinetics of binding suggest one class of sites also. In the case of these peptides, the affinities varied with the peptide, but in general they were lower (K_d varied from 10 nM in the case of C28F/A to 400 nM in the case of C23; see Table 2) than in the case of C28. C20 also showed an increase in fluorescence, but the data were better fitted assuming two classes of sites.

There are also peptides that do not fall under the previous categories: NΔ6C28 produced a decrease in fluorescence, similar to C28 (K_d = 3 nM), and at higher concentrations produced an increase in TA-CaM fluorescence ($K_d \simeq 230$ nM). Peptide C28W/A produced an increase in fluorescence followed by a smaller decrease at higher concentrations. Unfortunately, in the case of this peptide the fluorescence changes were too small to produce a good fit, but this complex behavior indicates more than one form of binding. Peptide C28V/A showed a similar behavior than C28, except that the affinity was lower (K_d = 50 nM), and the decrease in TA-CaM fluorescence upon binding was smaller than in the case of C28.

To learn more about the kinetics of binding of each of these peptides, we followed their binding to TA-CaM by

Table 2: Parameters for the Fittings of Different Models to TA-CaM Binding Data[a]

peptide	C28	C28NΔ6	C28W/A	C20	C23	C28F/A	C28V/A
model fitted	II	IV	IV	III	I	I	II
sum of squares	4.14×10^{-5}	7.7×10^{-5}	1.09×10^{-4}	1.03×10^{-4}	1.32×10^{-4}	1.265×10^{-4}	1.16×10^{-4}
k_1 ($s^{-1} M^{-1}$)	$(2.6 \pm 0.07) \times 10^8$	$(1.7 \pm 0.2) \times 10^8$	$(3.2 \pm 0.1) \times 10^9$	$(1.23 \pm 0.002) \times 10^9$	$(2.28 \pm 0.05) \times 10^8$	$(6.90 \pm 0.09) \times 10^8$	$(5.89 \pm 0.07) \times 10^8$
k_{-1} (s^{-1})	11.5 ± 0.5	31 ± 3	97 ± 2	16.34 ± 0.02	5.4 ± 0.1	0.39 ± 0.02	6.6 ± 0.2
k_2 (s^{-1})	4.1 ± 0.3	14 ± 1.1	24.4 ± 0.1		0.60 ± 0.04	1.46 ± 0.01	37 ± 0.3
k_{-2} (s^{-1})	2.14 ± 0.14	2.6 ± 0.1	9.75 ± 0.05		1.6 ± 0.1	0.48 ± 0.01	21.7 ± 0.1
k_3 (s^{-1})	2.7 ± 0.2	0.83 ± 0.05	3.78 ± 0.02				2.191 ± 0.005
k_{-3} (s^{-1})	>0.001	0.91 ± 0.02	0.09 ± 0.01				0.138 ± 0.004
k_4 ($s^{-1} M^{-1}$)		$(6 \pm 1) \times 10^8$	$(4.6 \pm 0.9) \times 10^9$	$(1.65 \pm 0.01) \times 10^8$			
k_{-4} (s^{-1})		1929 ± 345	4892 ± 55	10.49 ± 0.01			
k_5 ($s^{-1} M^{-1}$)				$(1.305 \pm 0.006) \times 10^4$			
k_{-5} (s^{-1})				1.16 ± 0.01			
r_{TA-CaM}	1	1	1	1	1	1	1
$r_{TA-CaM-C}$	1.416	1.078	1.64	1.03	1.75		1.68
$r_{TA-CaM-C\#}$	<0.1	0.637	1		1.60		1.40
$r_{TA-CaM-C*}$	<0.1	0.385	0.78				1.09
$r_{TA-CaM-Cd}$		<0.001	1.36	2.61			
$r_{TA-CaM-C2}$				>10			

[a] k_x refers to the forward rate constants for each of the steps in the models considered. k_{-x} refers to the reverse rate constants. $r_{TA-CaM-C}$ refers to the relative fluorescence of the species considered, taking the fluorescence of TA-CaM as 1.

stopped-flow techniques. Figure 4A shows the effects of N-terminal deletions. In this experiment, 17 nM TA-CaM was mixed with 200 nM of each of the peptides (final concentrations). When TA-CaM bound to the peptides with N-terminal deletions, TA-CaM fluorescence increased rapidly and then decreased more slowly, and the result was a net decrease in fluorescence in all cases. Figure 4B shows the changes in TA-CaM fluorescence upon binding to peptides with C-terminal deletions. A common feature is a fast phase in which fluorescence increased. Except for C20 and C22, this rapid increase was followed by a slower phase in which the fluorescence decreased. In the case of C20, two increasing exponential functions gave a better fit than one (see residuals in Figure 4C). A striking difference was that the end result of binding was a decrease in fluorescence for C28 and C25 but a net fluorescence increase for C20, C22, and C23. It should also be noted that the decreasing phase was fitted by one exponential in the case of C23, but two exponentials were needed for the decreasing phase of C28, C25, and all of the peptides with N-terminal deletions. Residuals are shown in Figure 4C, showing that the fit was much better when two decreasing exponentials were used for the decreasing phase.

Next, we compared the dissociation rates of the complexes between TA-CaM and each of these peptides. This was assessed by monitoring the fluorescence change when 17 nM CaM preincubated with 200 nM of each of the peptides was mixed with 2 μM unlabeled calmodulin. Results of the dissociation of the TA-CaM−C-terminal-deleted peptide complexes are shown in Figure 5. As expected, the dissociation of TA-CaM−peptide complexes, whose formation had led to an increase in fluorescence, led to a decrease in fluorescence (C20, C22, C23), and the dissociation of TA-CaM−peptide complexes, whose formation had led to a decrease in fluorescence, led to an increase in fluorescence (C25, C28, and all of the peptides with N-terminal deletions). The most interesting feature of these studies is that the complexes of TA-CaM with C20, C22, and C23 dissociated rapidly (with a half-time of about 30 s), while the dissociation of the complexes of TA-CaM with C28, C25, and the peptides with N-terminal deletions was extremely slow. The dissociation curves for C20, C22, and C23 were best fitted by the sum of two exponential functions (the dashed line shows that one exponential function did not give a plausible fit). For C20 the values of the apparent time constants were 0.22 ± 0.003 s^{-1} and 0.11 ± 0.01 s^{-1}, for C22 they were 0.13 ± 0.01 s^{-1} and 0.085 ± 0.005 s^{-1}, and for C23 these values were 0.25 ± 0.02 s^{-1} and 0.016 ± 0.001 s^{-1}. Due to the slow rate of the reaction, we did not obtain values for the dissociation rate constants of C28, C25, and the peptides with N-terminal deletions, but these can be estimated to be on the order of h^{-1}.

The next experiments analyzed the time course of TA-CaM binding at different concentrations of selected peptides. A wide variety of kinetic models were fitted to the results by using global nonlinear regression analysis. The models which gave the best fits followed four different schemes, which are presented in Figure 6. These models were developed on the basis of the model that we used previously to describe the interaction of C28 and CaM (*11*) to which we added the possibility of forming different abnormal complexes. The reader will notice that for different peptides some species designated with the same name fit to different fluorescence levels (e.g., the fluorescence level of TA-CaM−C_d is <0.001 for NΔ6C28 and 1.36 for C28W/A). Thus, these denominations indicate the same position in the kinetic scheme rather than the same structure. Many other schemes were also tested, but they gave fits too poor to be considered further.

Figure 7 shows the results of the binding of 17 nM TA-CaM to 50, 100, 200, and 400 nM C28. We had analyzed this peptide before (*11*), but since this analysis was done at a different temperature, we decided to repeat the analysis here. Nevertheless, the data obtained with C28 were fitted by the three-step model that we used before (*11*) (model II in Figure 6). Attempts to fit the data with simpler models did not give plausible fits. The rate constants that fitted the data are shown in Table 2. From the values of these rate

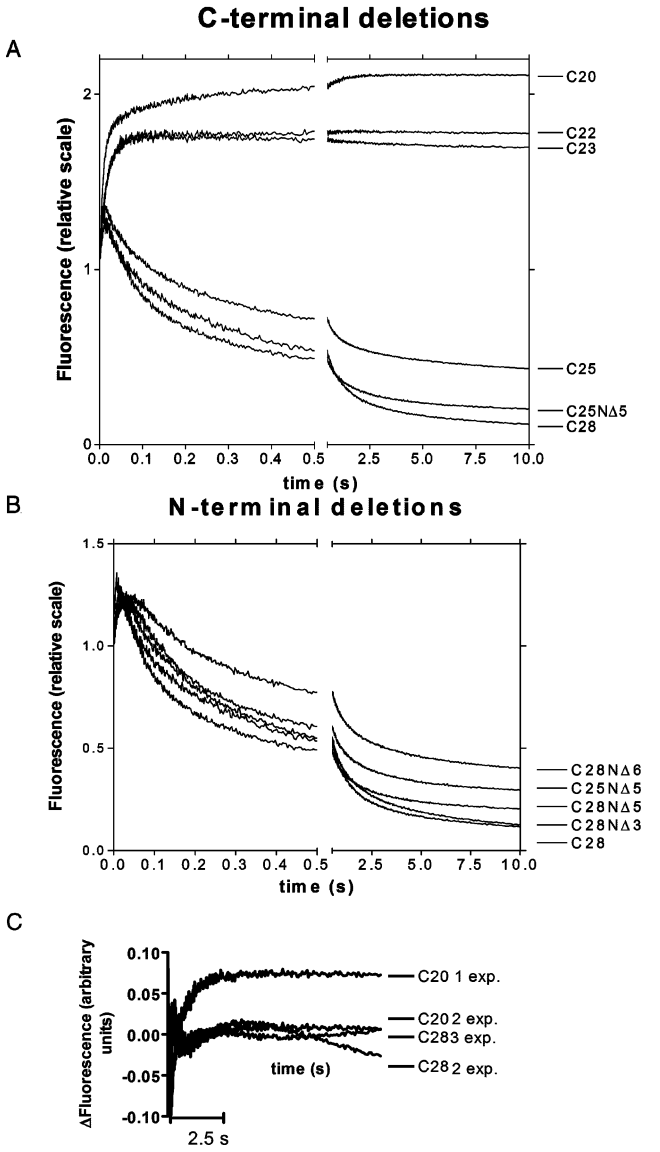

FIGURE 4: Fluorescence changes of TA-CaM upon binding to CaM-binding peptides from PMCA4b. Panel A: Peptides with C-terminal deletions. Panel B: Peptides with N-terminal deletions, except in the case of C25NΔ5, which has three residues deleted from the C-terminal end and five residues deleted from the N-terminal end. Panel C: Residual plot of the fit for peptides C20 considering one or two exponential functions and for peptide C28 considering two or three exponential functions. In all cases, the reaction started by mixing 17 nM TA-CaM with 200 nM peptide (final concentrations) in the media described in Experimental Procedures.

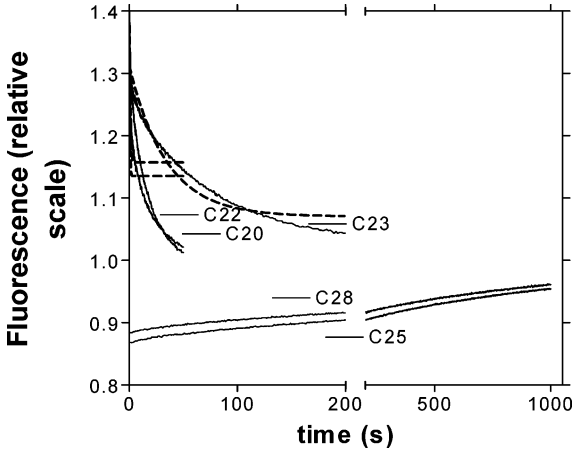

FIGURE 5: Dissociation of TA-CaM from C28, C25, C23, C22, and C20. 34 nM TA-CaM was premixed with 200 nM peptide, and at time = 0, 2 μM unlabeled CaM was added. Measurements were performed as described in Experimental Procedures.

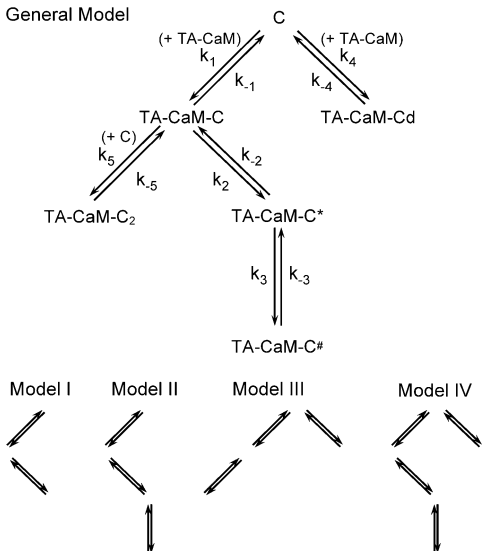

FIGURE 6: Basic reaction scheme and models derived from it. The rate constants shown in Table 2 were numbered from this scheme. The models shown were used for global nonlinear regression analysis fittings.

constants we inferred that the reaction proceeds first through a rapid and readily reversible step, followed by two steps that stabilize the complex. This conclusion confirmed our previous observations (*11*). Analysis of the kinetics of binding of C25, NΔ5C28, and NΔ5C25 to TA-CaM gave results similar to those obtained with C28 (not shown).

Then, we used global fitting to analyze the binding of C28NΔ6 to TA-CaM. Results are shown in Figure 8. As in the case of C28, the time course of TA-CaM binding shows a fast increase in fluorescence followed by a slower decrease, resulting in a net decrease in fluorescence. The results were fitted by a model which is similar to the one used for C28 but includes the possibility of the formation of an abnormal complex (model IV in Figure 6). The choice of the model was difficult, since in some experiments both model II and model IV fitted equally well the data, while in other experiments model IV gave a better fitting. However, model II does not explain the results of the equilibrium titrations (Figure 3), while model IV does. Therefore, we adopted model IV for the binding of C28NΔ6 to TA-CaM. The parameters for the fitting are shown in Table 2. The rate constants that were obtained are comparable to those obtained for C28, albeit 2−5 times slower. The rate constants for the formation of the abnormal complex suggest that its formation is a readily reversible reaction. Therefore, the effect of deleting six residues from the N-terminal end seems to consist of an increased possibility of complexes between TA-CaM and C28NΔ6 that are bound in the wrong orientation and, therefore, cannot be stabilized.

A characteristic of CaM-binding regions is the presence of a Trp residue in the N-terminal region of the peptide. It is generally believed that this Trp residue works as an anchor for the C-terminal lobe of CaM. It is known that when CaM binds to these peptides, there is a blue shift in the fluorescence of this Trp residue. When a 335 nm filter is used (that blocks light of wavelengths shorter than 335 nm), this shift

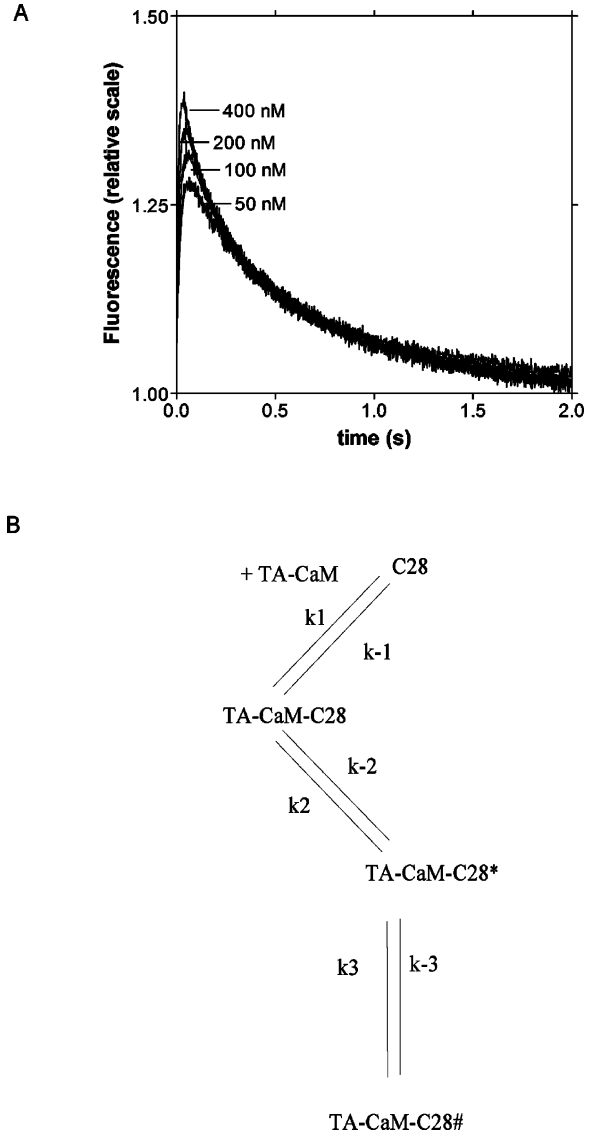

FIGURE 7: (A) Binding of C28 to TA-CaM at different C28 concentrations. The TA-CaM concentration was 17 nM. C28 concentrations were 50, 100, 200, and 400 nM. Changes in fluorescence were measured as described in Experimental Procedures. The fitting line represents $F(t) = r_{TA-CaM}[TA\text{-}CaM] + r_{TA-CaM-C28}[TA\text{-}CaM{-}C28] + r_{TA-CaM-C28*}[TA\text{-}CaM{-}C28^*] + r_{TA-CaM-C28\#}[TA\text{-}CaM{-}C28\#]$, where r denotes the relative quantum yield of each of the species considered. (B) Scheme of the model used to fit the data in panel A.

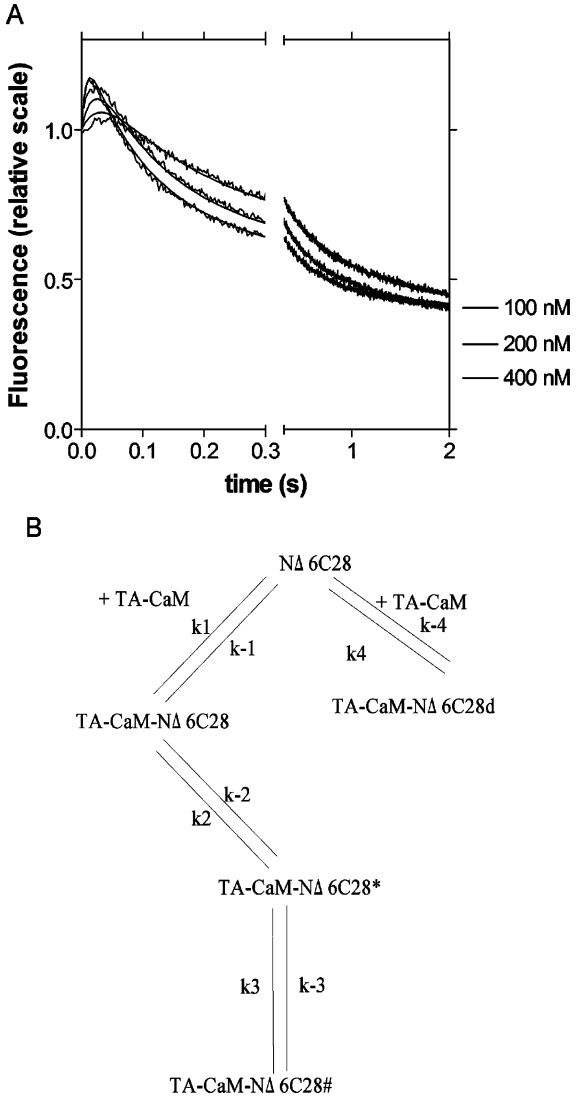

FIGURE 8: (A) Binding of C28NΔ6 to TA-CaM at different C28NΔ6 concentrations. The TA-CaM concentration was 17 nM. C28NΔ6 concentrations were 100, 200, and 400 nM. Changes in fluorescence were measured as described in Experimental Procedures. The fitting line represents $F(t) = r_{TA-CaM}[TA\text{-}CaM] + r_{TA-CaM-C28N\Delta6}[TA\text{-}CaM{-}C28N\Delta6] + r_{TA-CaM-C28N\Delta6*}[TA\text{-}CaM{-}C28N\Delta6^*] + r_{TA-CaM-C28N\Delta6\#}[TA\text{-}CaM{-}C28N\Delta6\#] + r_{TA-CaM-C28N\Delta6d}[TA\text{-}CaM{-}C28N\Delta6d]$, where r denotes the relative quantum yield of each of the species considered. (B) Scheme of the model used to fit the data in panel A.

can be seen as a decrease in fluorescence. To further explore the reaction of CaM with these CaM-binding peptides, we compared the changes in Trp fluorescence upon mixing C28 or C28NΔ6 and calmodulin. Results are shown in Figure 9A. C28 showed the expected decrease in fluorescence. On the contrary, C28NΔ6 showed an increase and then a decrease in fluorescence. When we performed emission scans of the complexes TA-CaM−C28 and TA-CaM−C28NΔ6, both complexes showed the blue shift characteristic of these complexes (λ_{max} about 335 nm compared to λ_{max} at 355 nm for the free peptides), but the fluorescence of the TA-CaM−C28NΔ6 complex was higher than the fluorescence of the TA-CaM−C28 complex (Figure 9B). These results indicate that the deletion of six residues from the N-terminal end of C28 alters somehow the environment of Trp_{1093} in the CaM−peptide complex.

Trp_{1093} is an important residue that has been shown to determine the rate of calmodulin dissociation from PMCA (*16*). It is conserved in calmodulin-binding motifs of targets that bind calmodulin in a Ca^{2+}-dependent manner (*17*). We studied the effect of mutating Trp_{1093} to Ala on the kinetics of TA-CaM binding. Results are shown in Figure 10. In Figure 3 we showed that binding of C28W/A showed little change in TA-CaM fluorescence. However, fast kinetic analysis shows that in fact there is a transient increase in fluorescence followed by a decrease of similar magnitude. At first sight, the kinetics of binding looks similar to that of C28: a phase in which fluorescence increases, followed by a decrease in fluorescence. However, as in the case of C28NΔ6, we had to include the possibility of formation of an abnormal complex to find a good fit to the data. Unlike the TA-CaM−C28NΔ6 dead-end complex, the TA-CaM−C28W/A abnormal complex showed higher fluorescence,

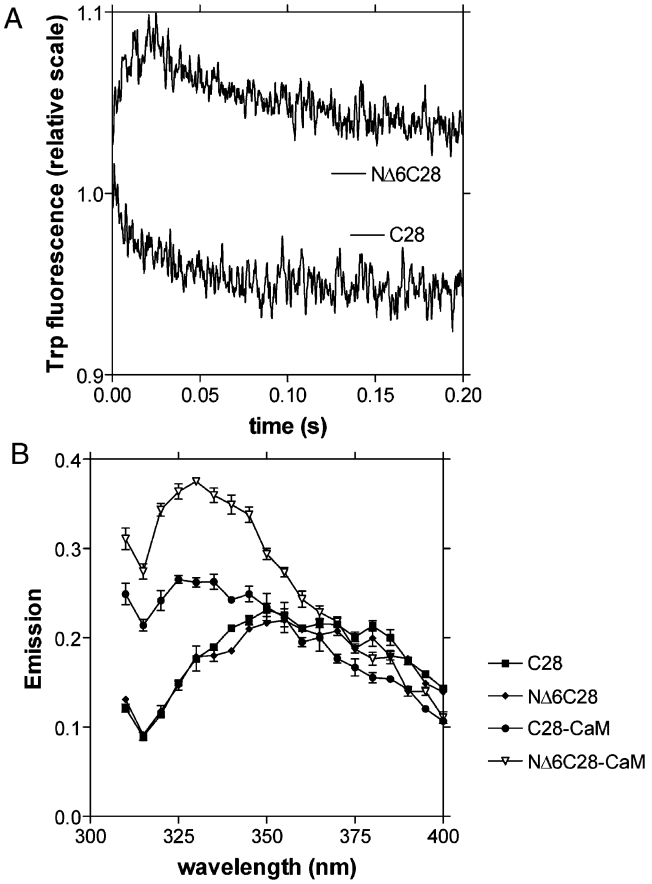

FIGURE 9: (A) Time course of Trp fluorescence change upon CaM binding to CaM-binding peptides C28 and C28NΔ6. At time = 0, 0.5 μM peptide was mixed with 2 μM CaM. Conditions are described in Experimental Procedures. (B) Emission scans of the free peptides and the peptides complexed with CaM. The excitation light was 295 nM.

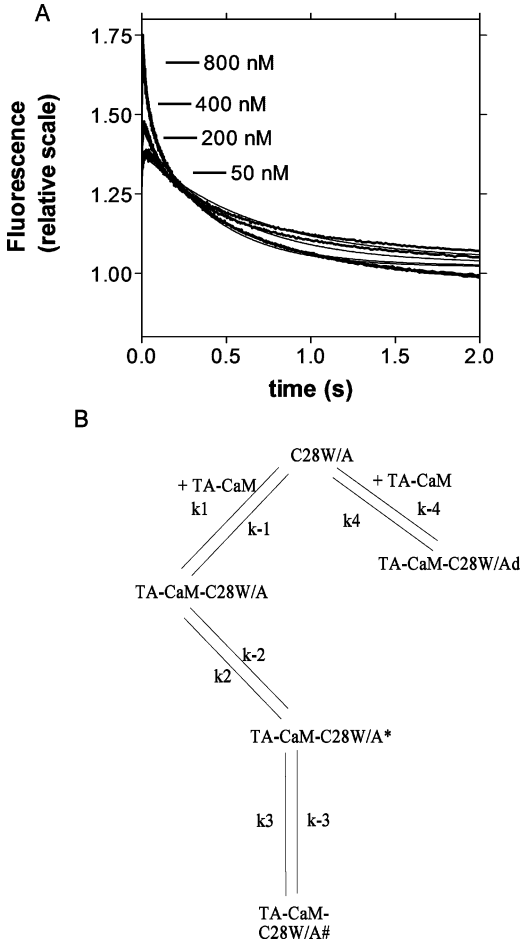

FIGURE 10: (A) Binding of C28W/A to TA-CaM at different C28W/A concentrations. The TA-CaM concentration was 34 nM. C28W/A concentrations were 50, 200, 400, and 800 nM. Changes in fluorescence were measured as described in Experimental Procedures. The fitting line represents $F(t) = r_{\mathrm{TA-CaM}}$[TA-CaM] + $r_{\mathrm{TA-CaM-C28W/A}}$[TA-CaM−C28W/A] + $r_{\mathrm{TA-CaM-C28W/A*}}$[TA-CaM−C28W/A*] + $r_{\mathrm{TA-CaM-C28W/A\#}}$[TA-CaM−C28W/A#] + $r_{\mathrm{TA-CaM-C28W/Ad}}$[TA-CaM−C28W/Ad], where r denotes the relative quantum yield of each of the species considered. (B) Scheme of the model used to fit the data in panel A.

indicating that the abnormal complexes are different. The parameters of the fitting are shown in Table 2. The most striking observation is that the rate constants for both the formation and dissociation of the first complex and the abnormal complex are very fast, suggesting that the absence of Trp_{1093} allows for rapid formation of TA-CaM−C28W/A complexes but that these complexes are very unstable. Interestingly, a W_{1093}/A mutant of PMCA4b showed faster activation by CaM and inactivation by CaM removal (*16*).

Next, we examined the binding of TA-CaM to peptides with C-terminal deletions. Since C25 produced a pattern similar to the full-length C28, and C22 was similar to C23, we focused our analysis on C20 and C23. Binding of C20 to TA-CaM produced an increase in fluorescence that is more pronounced at higher C20 concentrations (Figure 11). The results are fitted by a model in which TA-CaM binds to C20 and then there is an unique conversion step. In order for the model to fit, it is necessary to propose that C20 binds to TA-CaM in other ways but with lower affinity. That is that C20 and TA-CaM can bind in the wrong orientation and that TA-CaM can possibly bind two C20 peptides. The parameters of the fitting (Table 2) indicate that the binding proceeds through a fairly rapid initial step, readily reversible. The ratio k_{-4}/k_4 and k_{-5}/k_5 indicated K_ds for the dead-end complexes of 63 nM and 89 μM, respectively. Compared to a K_d of 13 nM for the TA-CaM−C20 complex (from k_{-1}/k_1), this indicates that the abnormal complexes are formed with low affinity.

We also analyzed the kinetics of binding of C23, the longest peptide with C-terminal deletions that produces a net increase in fluorescence upon binding of TA-CaM (Figure 12). The model that fitted the results best was a two-step model (model I in Figure 5). Additional steps did not improve the fitting significantly. Unlike C20, there was no need to propose the existence of abnormal complexes or ternary complexes between calmodulin and C23.

Since the effect of deleting Phe_{1110} is very dramatic, both on the forward and on the reverse reaction (see Figures 4, 5, and 12), we decided to test the kinetics of binding of TA-CaM to a peptide in which Phe_{1110} was replaced by Ala (C28F/A). The results of this experiment are shown in Figure 12. As is the case for C23, binding of TA-CaM to C28F/A fitted to a two-step model. The pattern of the reaction also resembles C23 (compare Figure 12 with Figure 13). The parameters for the kinetics of this reaction are shown in Table 2. Since in other CaM-binding domains the residue that is in the position of Val_{1107} is proposed to be a second anchor that binds to the N-terminal lobe of CaM, we also tested the

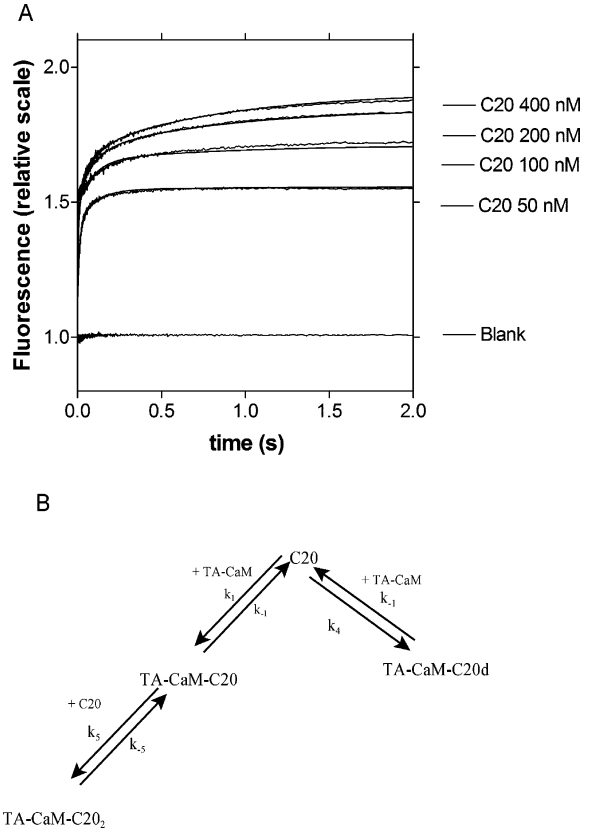

FIGURE 11: (A) Binding of C20 to TA-CaM at different C20 concentrations. The TA-CaM concentration was 34 nM. C20 concentrations were 0, 50, 100, 200, and 400 nM. Changes in fluorescence were measured as described in Experimental Procedures. The fitting line represents $F(t) = r_{TA-CaM}[TA\text{-}CaM] + r_{TA-CaM-C20}[TA\text{-}CaM-C20] + r_{TA-CaM-C20_2}[TA\text{-}CaM-C20_2] + r_{TA-CaM-C20d}[TA\text{-}CaM-C20d]$, where r denotes the relative quantum yield of each of the species considered. (B) Scheme of the model used to fit the data in panel A.

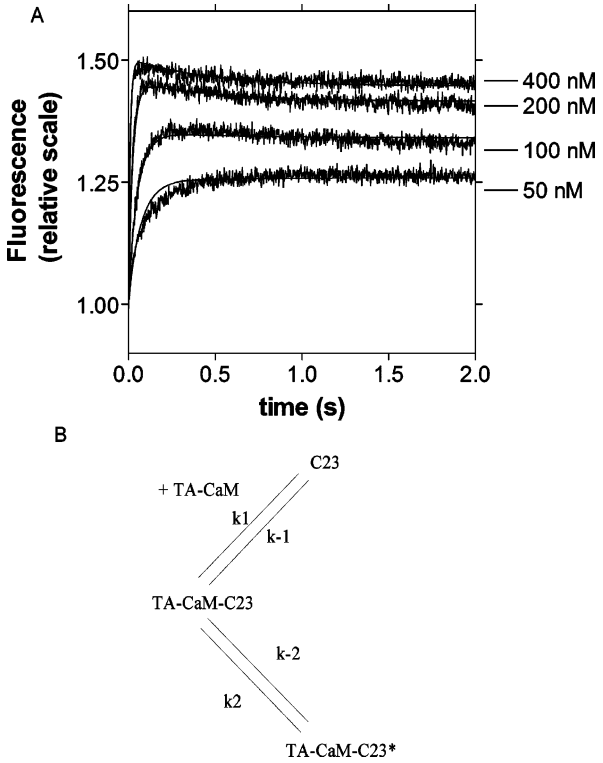

FIGURE 12: (A) Binding of C23 to TA-CaM at different C23 concentrations. The TA-CaM concentration was 17 nM. C23 concentrations were 50, 100, 200, and 400 nM. Changes in fluorescence were measured as described in Experimental Procedures. The fitting line represents $F(t) = r_{TA-CaM}[TA\text{-}CaM] + r_{TA-CaM-C23}[TA\text{-}CaM-C23] + r_{TA-CaM-C23*}[TA\text{-}CaM-C23*]$, where r denotes the relative quantum yield of each of the species considered. (B) Scheme of the model used to fit the data in panel A.

effect of mutating that residue to Ala (C28V/A) on the kinetics of binding of TA-CaM. The results of such experiment are shown in Figure 14. In this case, the results are fitted by a three-step model similar to the one used for C28. The major difference is that the last intermediate in the binding reaction shows higher fluorescence than in the case of TA-CaM−C28.

Figure 15 compares the dissociation reaction of the complexes between TA-CaM and C28, C28F/A, and C28V/A. The dissociation rates of the TA-CaM−C28 and TA-CaM−C28V/A complexes are difficult to measure because they are very slow. However, it is evident that the dissociation of the TA-CaM−C28F/A complex is much faster than the other two complexes. This experiment confirms that Phe_{1110} is very important for the stabilization of the CaM−C28 complex.

DISCUSSION

Both the inhibition by competition experiments and the kinetic data of TA-CaM binding show that the limit sequence for CaM binding is from I_{1091} to F_{1110}. Peptides that did not include the residues comprised in that sequence showed lower K_{eq} as competitive inhibitors in CaM activation experiments. Titration experiments using TA-CaM led to similar results. They also failed to reproduce the characteristics of TA-CaM binding to C28. Taken together, these results point at the sequence I_{1091}LWFRGLNRIQTQIKVVKAF$_{1110}$ as the minimal sequence that reproduces all the characteristics of CaM binding to C28.

It should be pointed out that the competition experiments, since they are based on the ratio of affinities of CaM for the peptides and for PMCA, do not estimate well K_{eq}s lower than 0.5 nM (unpublished observations). Also, since the titrations of TA-CaM were performed at 34 nM TA-CaM, these titrations do not estimate very well extremely high affinities but are useful for comparison purposes. An alternative approach consists of calculating K_ds for the different complexes from the rate constants shown in Table 2. When we used this procedure, the K_d for the TA-CaM−C28 complex was estimated to be around 9 pM, for TA-CaM−C23 was 0.6 nM, and for C20 was 13 nM. This emphasizes the high affinity of the TA-CaM−C28 complex and the differences in affinity between the three peptides.

Deletions of the five first residues in the N-terminal end of C28 are silent, suggesting that these residues do not have an important role during CaM binding. This is consistent with the published structure of the CaM−C20 complex in which these residues have very few contacts (*18*). Deletion of six residues, including I_{1091}, decreases the affinity for CaM 5-fold. When association and dissociation of TA-CaM were tested, binding of C28NΔ6 to TA-CaM produced a decrease in TA-CaM fluorescence, and dissociation of C28NΔ6 was slow as in the case of C28. However, the association data were not fitted by a linear three-step model. It was necessary

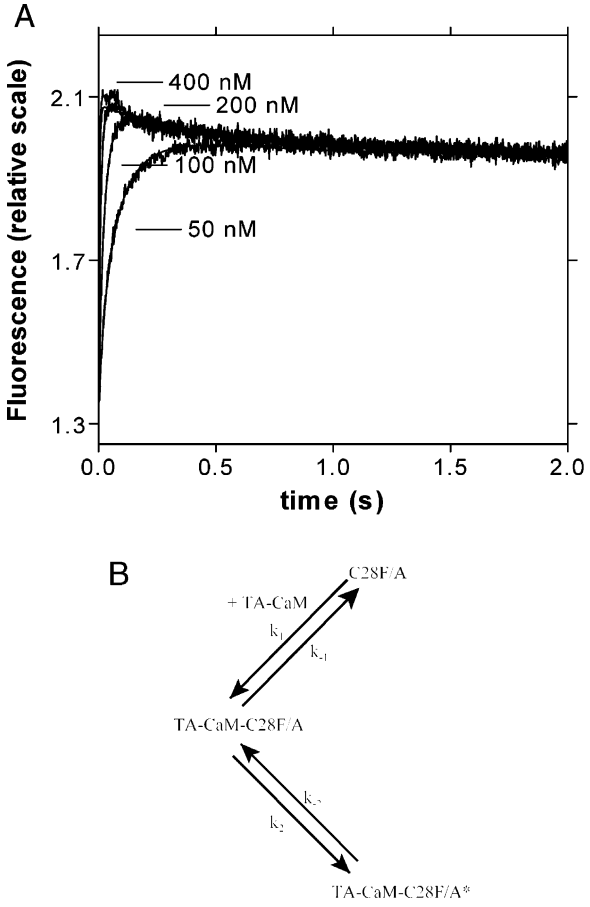

FIGURE 13: (A) Binding of C28F/A to TA-CaM at different C28F/A concentrations. The TA-CaM concentration was 17 nM. C28F/A concentrations were 50, 100, 200, and 400 nM. Changes in fluorescence were measured as described in Experimental Procedures. The fitting line represents $F(t) = r_{TA-CaM}[TA\text{-}CaM] + r_{TA-CaM-C28F/A}[TA\text{-}CaM{-}C28F/A] + r_{TA-CaM-C28F/A*}[TA\text{-}CaM{-}C28F/A^*]$, where r denotes the relative quantum yield of each of the species considered. (B) Scheme of the model used to fit the data in panel A.

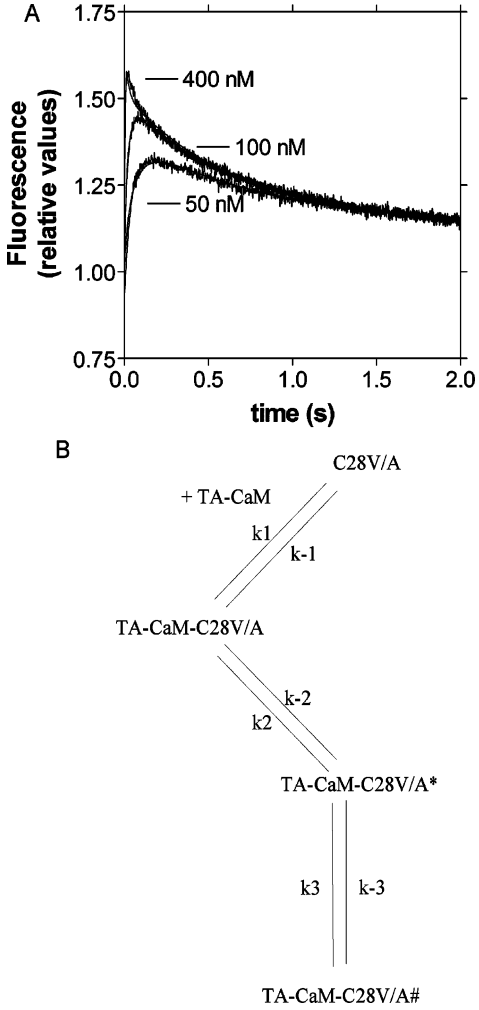

FIGURE 14: (A) Binding of C28V/A to TA-CaM at different C28V/A concentrations. The TA-CaM concentration was 17 nM. C28V/A concentrations were 50, 100, and 400 nM. Changes in fluorescence were measured as described in Experimental Procedures. The fitting line represents $F(t) = r_{TA-CaM}[TA\text{-}CaM] + r_{TA-CaM-C28V/A}[TA\text{-}CaM{-}C28V/A] + r_{TA-CaM-C28V/A*}[TA\text{-}CaM{-}C28V/A^*] + r_{TA-CaM-C28V/A\#}[TA\text{-}CaM{-}C28V/A\#]$, where r denotes the relative quantum yield of each of the species considered. (B) Scheme of the model used to fit the data in panel A.

to introduce the formation of an abnormal complex (possibly a complex with TA-CaM and peptide aligned in the wrong orientation) to fit the data. Also, the changes in Trp fluorescence were different: together with the blue shift common to all of the tested peptides when binding to CaM, C28NΔ6 shows also an increase in fluorescence, and equilibrium titrations showed indications of more than one type of binding. It is possible that this increase is related to peptides binding to CaM in the wrong orientation also. Interestingly, the C28W/A peptide, in which W_{1093} was changed to A, also fitted to a model involving an abnormal complex, although in this case the fluorescence of the abnormal complex was higher than for the one formed by C28NΔ6, indicating that the characteristics of the abnormal complexes were different for C28W/A and C28NΔ6. In either case, the results of equilibrium titrations indicated more than one form of binding. A possible explanation is the formation of CaM−peptide complexes in the wrong orientation. The occurrence of CaM−peptide complexes formed in the wrong orientation was previously suggested in ref *10* for binding of CaM to α-CaM kinase II. Moreover, structural evidence has been recently presented for alternative orientations in the case of the CaM−mellitin complex (*19*). It is interesting to note that, in the case of PMCA4b, only peptides

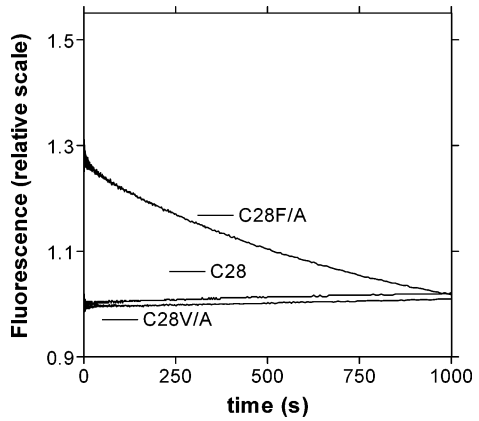

FIGURE 15: Comparison of the time course of dissociation of C28−TA-CaM, C28V/A−TA-CaM, and C28F/A−TA-CaM complexes. 34 nM TA-CaM was premixed with 200 nM peptide, and at time = 0, 2 μM unlabeled CaM was added. Measurements were performed as described in Experimental Procedures.

that are very short (C20, NΔ6C28) or that lack the anchoring W residue are able to form abnormal complexes.

A general statement that can be made about the interaction of these PMCA-derived peptides with TA-CaM is that it is characterized by a first step that is fast and reversible. This step may (all of the peptides except C20) or may not (C20) be followed by other steps that stabilize the complex. On the basis of the NMR structure of the C20−CaM complex (*18*), the first step most probably represents the interaction of the N-terminal region of the peptide with the C-terminal lobe of CaM. The fact that in the case of C28W/A this first step is extremely fast suggests that burying the W residue slows down the first interaction between the C-terminal lobe of TA-CaM and the calmodulin-binding region. The complex C28W/A−TA-CaM dissociates with a half-time of about 8 s (results not shown). When tested in the whole protein, the W_{1093}/A mutation resulted in a PMCA with higher activity in the absence of CaM, a faster activation by CaM, but also a much faster dissociation rate for CaM (*16*). This evidence confirms that Trp_{1093} plays an important role in stabilizing the complex between CaM and PMCA.

Deletions on the C-terminal end of this CaM-binding region provided a very interesting insight on this reaction: our results show that when peptides that lack the five C-terminal residues (C23 and shorter) bind to TA-CaM, the fluorescence of TA-CaM increases, while when peptides that include F_{1110} bind to TA-CaM, the fluorescence of the probe shows a rapid increase followed by a slower decrease, and the net result is a decrease in fluorescence. Also, C23 and shorter peptides show a relatively fast dissociation rate from TA-CaM, while C25 and longer peptides show a very slow dissociation rate from TA-CaM. Taken together, these results suggest that CaM can adopt a collapsed structure around peptides that include F_{1110}, binding both lobes of CaM, while peptides that do not include this residue can only bind one lobe, or if they bind two, they do so in an incomplete manner. Based on our data and the structural information available (see below), it is possible to speculate that the three-step model for binding of C28 to TA-CaM corresponds to fast binding of the C-terminal lobe of CaM to the N-terminal region of C28, binding of the N-terminal lobe of CaM to the C-terminal region of the peptide, and CaM collapse around the peptide. Although more evidence is needed, this idea is compatible with the present data.

The importance of F_{1110} was confirmed by experiments in which this residue was replaced by A (peptide C28F/A). In such case, the pattern of TA-CaM binding resembled the one observed for C23, both in dissociation and in association of TA-CaM. Substitution of V_{1107} for A (peptide C28V/A) also produced changes in the pattern of binding, but not as pronounced as in the case of F_{1110}. In fact, although with different values for the relative fluorescence of the species and rate constants, it was necessary to fit the data with a three-step model for both C28 and C28V/A, but only two steps were needed for C28 F/A. It is interesting to compare these results with some structural data already known.

An NMR structure of a CaM−C20 complex (C20 lacks the eight C-terminal residues of C28, including V_{1107} and F_{1110}) shows that the C-terminal lobe of CaM has a very strong contact with Trp_{1093}, but there is no contact with the N-terminal lobe, and CaM is in an extended conformation (*18*). However, X-ray scattering experiments show that in a complex of CaM with a peptide similar to C28 but lacking the four N-terminal residues (in the nomenclature used here, C28NΔ4) CaM collapses around the peptide (*20*). Our interpretation is consistent with these structural data.

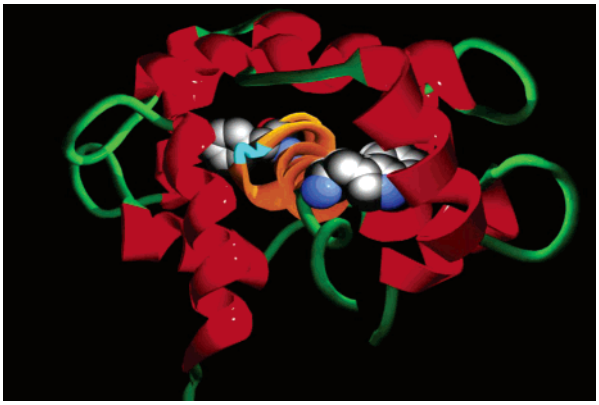

FIGURE 16: A model of the CaM−C28 complex, based on known structures as described in Experimental Procedures and the data from this paper. Helical regions of calmodulin are in red, helical regions of C28 are in orange, and all coiled regions are in green except that the short coiled region in the middle of the C28 helix is highlighted in cyan. The two anchor residues of C28 are shown in space-filling form; the Trp is at the end near the viewer and the Phe at the far end.

Sequence motifs for Ca^{2+}-dependent CaM binding have been classified into 1−5−10 and 1−8−14 groups, depending on the periodicity of hydrophobic residues (*17*). The first and third hydrophobic residues bind to the hydrophobic pocket in the C-terminal and N-terminal lobe of CaM, respectively. On the basis of the results of this paper, we suggest that, in the case of PMCA4b, the classification is 1−8−18.

In the structure of the complex between myosin light chain kinase peptide and calmodulin, the distance between the α carbons of W1 and F14 is 19.7 Å, and the peptide is arranged in a nearly perfect helix between them (*21*). In the complex of nitric oxide synthase peptide with calmodulin, the helix is slightly unwound and extended, giving a distance of 20.8 Å between F1 and L14 ((*22*). On these precedents, we expected V14 to be the second anchor residue in the complex of PMCA peptide with calmodulin, with a distance of about 20 Å between the two anchor residues. The results of this study surprisingly disclosed that F18 is the second anchor residue rather than V14. In order for 18 residues to fit between the two anchor points of a collapsed calmodulin structure like that of MLCK or NOS, the helix would need to be shortened either by bending or by untwisting. The studies reported here indicate the calmodulin is undergoing a substantial conformational change indicating a collapse. It follows that the final distance between the lobes of calmodulin must be greater than is the case for MLCK or NOS or that shortening of the helix must occur, or some combination of both.

Figure 16 shows the result of a study in which a model of the C28−calmodulin complex was made on the basis of the known structures of other peptide−calmodulin complexes. In this model, the helix was shortened by untwisting and looping a short stretch of helix, highlighted in bright blue in Figure 16. Clearly, other means of shortening the helix might accomplish the same result, but we conclude that a shortening of the helix or a less profound collapse of calmodulin is necessary to harmonize the 18-residue spacing of the anchor residues with the other data.

This study provides a detailed insight on the relevant PMCA4b residues for CaM binding. The functional importance of this study is highlighted by a paper in which CaM activation was analyzed in different truncated mutants of PMCA4b. In agreement with the results reported here, CaM activated with high affinity all of the mutants that contained the C28 region. However, a mutant that was truncated after K_{1106} (as is the case of the C20 peptide) showed decreased affinity for CaM (*23*).

In humans, PMCA is encoded by four genes, and alternate splicing produces more than 20 isoforms (reviewed in ref *24*). All four PMCA genes and splicing variants contain the same first 18 residues of the C28 CaM-binding region. Alternate splicing at site "C" of all four PMCAs occurs after the codon encoding Q1104, which corresponds to Q18 of peptide C28 (Figure 1). We have previously shown that alternative splicing at site C affects the steady-state affinity for CaM (*25*) and the rate of activation by Ca−CaM, as well as the rate of inactivation of the PMCA−Ca−CaM complex induced by removal of Ca and/or CaM (*2*). In a recent investigation by our laboratory, the activation of PMCA4b by CaM or TA-CaM was shown to occur on a time scale consistent with the later stages of decreasing fluorescence of TA-CaM, suggesting that initial interaction with CaM, as evidenced by the rapid increase in TA-CaM fluorescence, is not sufficient to activate PMCA (*11*). The data presented here suggest that diversity of PMCA genes and alternate splicing generate a host of PMCAs that should bind the C-terminal domain of CaM with similar affinity but that interaction with the N-terminal domain of CaM and subsequent collapse of CaM differ, in part, due to sequence variation induced by alternative splicing.

While this investigation defines the boundaries of the CaM-binding region of PMCA, it must be noted that the CaM-binding region also serves as an autoinhibitor of PMCA (*7*). Thus, the kinetics of activation and inactivation of PMCA involve the kinetics of binding the autoinhibitory sequence to the catalytic core of PMCA in addition to the kinetics of CaM binding. The autoinhibitory properties of CaM-binding regions of PMCAs are the subject of current and future kinetic studies.

ACKNOWLEDGMENT

We thank Katalin Török and Richard Thorogate (Department of Pharmacology and Clinical Pharmacology, St. George Hospital Medical School) for the generous provision of TA-CaM and for extremely helpful discussions.

REFERENCES

1. Enyedi, Á., Flura, M., Sarkadi, B., Gardos, G., and Carafoli, E. (1987) The maximal velocity and the calcium affinity of the red cell calcium pump may be regulated independently, *J. Biol. Chem. 262*, 6425−6430.
2. Caride, A. J., Elwess, N. L., Verma, A. K., Filoteo, A. G., Enyedi, Á., Bajzer, Z., and Penniston, J. T. (1999) The rate of activation by calmodulin of isoform 4 of the plasma membrane Ca^{2+} pump is slow and is changed by alternative splicing, *J. Biol. Chem. 274*, 35227−35232.
3. Caride, A. J., Filoteo, A. G., Penheiter, A. R., Pászty, K., Enyedi, Á., and Penniston, J. T. (2001) Delayed activation of the plasma membrane calcium pump by a sudden increase in Ca^{2+}: Fast pumps reside in fast cells, *Cell Calcium 30*, 49−57.
4. Caride, A. J., Penheiter, A. R., Filoteo, A. G., Bajzer, Z., Enyedi, Á., and Penniston, J. T. (2001) The plasma membrane calcium pump displays memory of past calcium spikes: Differences between isoforms 2b and 4b, *J. Biol. Chem. 276*, 39797−39804.
5. Bautista, D. M., Hoth, M., and Lewis, R. S. (2002) Enhancement of calcium signalling dynamics and stability by delayed modulation of the plasma membrane calcium pump in human T cells, *J. Physiol. 541*, 877−894.
6. James, P., Maeda, M., Fischer, R., Verma, A. K., Krebs, J., Penniston, J. T., and Carafoli, E. (1988) Identification and primary structure of a calmodulin-binding domain of the Ca^{2+} pump of human erythrocytes, *J. Biol. Chem. 263*, 2905−2910.
7. Enyedi, Á., Vorherr, T., James, P., McCormick, D. J., Filoteo, A. G., Carafoli, E., and Penniston, J. T. (1989) The calmodulin binding domain of the plasma membrane Ca^{2+} pump interacts both with calmodulin and with another part of the pump, *J. Biol. Chem. 264*, 12313−12321.
8. Enyedi, Á., Verma, A. K., Filoteo, A. G., and Penniston, J. T. (1993) A highly active truncated mutant of the plasma membrane Ca^{2+} pump, *J. Biol. Chem. 268*, 10621−10626.
9. Török, K., and Trentham, D. R. (1994) Mechanism of 2-chloro-(ϵ-amino-Lys75)-[6-[4-(*N*,*N*- diethylamino)phenyl]-1,3,5-triazin-4-yl]calmodulin interactions with smooth muscle myosin light chain kinase and derived peptides, *Biochemistry 33*, 12807−12820.
10. Török, K., Tzortzopoulos, A., Grabarek, Z., Best, S. L., and Thorogate, R. (2001) Dual effect of ATP in the activation mechanism of brain Ca^{2+}/calmodulin-dependent protein kinase II by Ca^{2+}/calmodulin, *Biochemistry 40*, 14878−14890.
11. Penheiter, A. R., Bajzer, Z., Filoteo, A. G., Thorogate, R., Torok, K., and Caride, A. J. (2003) A model for the activation of plasma membrane calcium pump isoform 4b by calmodulin, *Biochemistry 42*, 12115−12124.
12. Penniston, J. T., Filoteo, A. G., McDonough, C. S., and Carafoli, E. (1988) Purification, Reconstitution and Regulation of Plasma Membrane Ca^{2+} Pumps, *Methods Enzymol. 157*, 340−351.
13. Niggli, V., Adunyah, E. S., Penniston, J. T., and Carafoli, E. (1981) Purified Ca^{2+}-Mg^{2+} ATPase of the erythrocyte membrane: Reconstitution and effect of calmodulin and phospholipids, *J. Biol. Chem. 256*, 395−401.
14. Torok, K., Cowley, D. J., Brandmeier, B. D., Howell, S., Aitken, A., and Trentham, D. R. (1998) Inhibition of calmodulin-activated smooth-muscle myosin light-chain kinase by calmodulin-binding peptides and fluorescent (phosphodiesterase-activating) calmodulin derivatives, *Biochemistry 37*, 6188−6198.
15. Kuzmic, P. (1996) Program DYNAFIT for the Analysis of Enzyme Kinetic Data: Application to HIV Proteinase, *Anal. Biochem. 237*, 260−273.
16. Penheiter, A. R., Caride, A. J., Enyedi, Á., and Penniston, J. T. (2002) Tryptophan^{1093} is largely responsible for the slow off rate of calmodulin from PMCA 4b, *J. Biol. Chem. 277*, 17728−17732.
17. Rhoads, A. R., and Friedberg, F. (1997) Sequence motifs for calmodulin recognition, *FASEB J. 11*, 331−340.
18. Elshorst, B., Hennig, M., Forsterling, H., Diener, A., Maurer, M., Schulte, P., Schwalbe, H., Griesinger, C., Krebs, J., Schmid, H., Vorherr, T., and Carafoli, E. (1999) NMR solution structure of a complex of calmodulin with a binding peptide of the Ca^{2+} pump, *Biochemistry 38*, 12320−12332.
19. Schulz, D. M., Ihling, C., Clore, G. M., and Sinz, A. (2004) Mapping the topology and determination of a low-resolution three-dimensional structure of the calmodulin-melittin complex by chemical cross-linking and high-resolution FTICRMS: Direct demonstration of multiple binding modes, *Biochemistry 43*, 4703−4715.
20. Kataoka, M., Head, J. F., Vorherr, T., Krebs, J., and Carafoli, E. (1991) Small-angle X-ray scattering study of calmodulin bound to two peptides corresponding to parts of the calmodulin-binding domain of the plasma membrane Ca^{2+} pump, *Biochemistry 30*, 6247−6251.
21. Ikura, M., Clore, G. M., Gronenborn, A. M., Zhu, G., Klee, C. B., and Bax, A. (1992) Solution structure of a calmodulin-target peptide complex by multidimensional NMR, *Science 256*, 632−638.
22. Aoyagi, M., Arvai, A. S., Tainer, J. A., and Getzoff, E. D. (2003) Structural basis for endothelial nitric oxide synthase binding to calmodulin, *EMBO J. 22*, 766−775.

23. Verma, A. K., Enyedi, Á., Filoteo, A. G., and Penniston, J. T. (1994) Regulatory region of plasma membrane Ca^{2+} pump. 28 residues suffice to bind calmodulin but more are needed for full auto-inhibition of the activity, *J. Biol. Chem. 269*, 1687−1691.
24. Strehler, E. E., and Zacharias, D. A. (2001) Role of alternative splicing in generating isoform diversity among plasma membrane calcium pumps, *Physiol. Rev. 81*, 21−50.
25. Enyedi, Á., Verma, A. K., Heim, R., Adamo, H. P., Filoteo, A. G., Strehler, E. E., and Penniston, J. T. (1994) The Ca^{2+} affinity of the plasma membrane Ca^{2+} pump is controlled by alternative splicing, *J. Biol. Chem. 269*, 41−43.

BI0488552